An Empirical Identification Method of Gaussian Blur Parameter for Image Deblurring

Fen Chen, *Member, IEEE*, and Jianglin Ma

***Abstract*—In this paper, we propose an empirical identification method of the Gaussian blur parameter for image deblurring. The parameter estimate is chosen from a collection of candidate parameters. The blurred image is restored by these candidate parameters under the assumption that the candidate is equal to the true value. The estimate is selected to be at the maximum point of the differential coefficients of restored image Laplacian L1 norm curve. Experimental results are presented to demonstrate the performance of the proposed method.**

***Index Terms*—Boundary conditions, Gaussian blur, image deblurring, parameter identification, point spread function (PSF).**

I. Introduction

In many imaging systems, the observed images would unfortunately suffer blurring due to many degradations such as defocusing, diffraction, relative motion between the camera and the scene, and in some cases, atmospheric turbulence. The goal of image restoration is to recover the scene closely from the degraded image. In many applications, the degradation procedure of imaging system could be modeled as the result of a convolution with a linear shift-invariant low-pass filter h. This low-pass filter h is often called point spread function (PSF).

$$g(x,y)=\sum_{k=1}^{M}\sum_{l=1}^{N} f(k,l)h(x-k,y-l)+\xi(x,y). \quad (1)$$

In (1), $\xi(x,y)$ is the noise introduced in the procedure of image acquisition, and it is generally assumed to be zero-mean additive white Gaussian noise with variance σ_n^2. Equation (1) could be expressed in matrix-vector formulation

$$\mathbf{g}=\mathbf{H}\mathbf{f}+\mathbf{n} \quad (2)$$

where $\mathbf{g}$, $\mathbf{f}$ and $\mathbf{n}$ are the observed image, original image, and additive white Gaussian noise, respectively, ordered lexicographically by stacking the rows of each image into a vector. $\mathbf{H}$ denotes the PSF h as a linear convolution operator. Three forms of PSF models are commonly used in image restoration: the defocus blur, the motion blur, and the Gaussian blur.

Classical restoration methods require complete knowledge of the blur PSF prior to restoration [2], [3], [10], [11]. However, in many applications, the PSF is often unknown *a priori* or is known only within a parameter due to various practical constraints. As the knowledge is rarely available, identification of the PSF from only the observed degraded images has been of great interest. A number of techniques have been proposed to address this problem. Gennery [5] suggested identifying zeros in the frequency spectrum of the blurred image. However, in noisy conditions, finding spectral zeros is more or less impossible as they are covered by the noise power spectrum. Bispectrum [4] is proposed as an alternate method to reduce the effects of noise. But, these methods are not suited for Gaussian blur parameter identification, because there are no regular zeros in its frequency content as there are in defocus blur and motion blur. Another blur identification method by residual spectral matching is proposed by Savakis *et al.* [21], but it needs the knowledge of the noise variance and the original image spectrum which are usually hard to accurately estimate. In other methods [12], [13], [20], the original image has been modeled as an autoregressive (AR) process, and the blur as a moving average (MA) process. With the image and blur modeled in this way, the blur identification problem becomes a matter of determining the parameters of an ARMA model. The parameters can be estimated by the maximum-likelihood (ML) [13], the expectation maximization (EM) [12] or the generalized cross validation (GCV) [20] method. However, their performance suffers from the possible poor convergence to local minima during the maximization process. Another limitation of them is that the computational load is heavy. Li [14], [15] proposed identifying the blurring parameter with kurtosis minimization. The deblurred image with the smallest kurtosis is chosen as the final restored image, and the corresponding parameter is regarded as the identified blurring parameter. However, the estimation error of this method is sometimes large.

In some applications, such as in remote sensing, the PSF of atmospheric turbulence is often modeled as Gaussian blur.

$$h(x,y)=\begin{cases} K\exp\left\{-\frac{(x^2+y^2)}{2\sigma^2}\right\}, & (x,y)\in C \\ 0, & \text{elsewhere} \end{cases} \quad (3)$$

where x and y are the horizontal and vertical space variables; σ is the standard deviation, which parameterizes the severity of the blur; C is the region of support and K is a normalization constant. Thus, the Gaussian PSF could be characterized by a single parameter σ. In our experiment, the support region C is

Manuscript received May 31, 2008; accepted January 19, 2009. First published March 21, 2009; current version published June 17, 2009. The associate editor coordinating the review of this paper and approving it for publication was Prof. James Lam. This work was supported by the China NSF by Grant 40801171.

F. Chen is with the College of Automation, University of Electronic Science and Technology of China, Chengdu, 610054, China (e-mail: chenfen@uestc.edu.cn).

J. Ma is with the Department of Geography, Faculty of Sciences, Vrije Universiteit Brussel, Brussel, 1050, Belgium (e-mail: jianglin.ma@vub.ac.be).

Digital Object Identifier 10.1109/TSP.2009.2018358

set as $[-3\sigma, 3\sigma]$, because, for a Gaussian function, almost 99.7% of its energy is concentrated within.

As far as we know, there are less practically effective parameter identification methods for Gaussian blur than for defocus blur and motion blur. The reason may be that there are no zeros in its frequency content, and an inaccurate estimated parameter would not cause such a severely unacceptable result as defocus blur and motion blur, so the restored images are not easily distinguishable.

In this paper, a new simple empirical identification method of Gaussian blur parameter is proposed based on the observations of the restored image's second derivatives L1 norm curve. The PSF estimate is chosen from a collection of candidate parameters. After performing the deblurring for each candidate parameter under the assumption that it is the true PSF, the L1 norm of its corresponding restored image's second derivatives is computed. An exhaustive search is performed throughout the candidates' L1 norm curve and the PSF estimate is chosen at the maximum point of this curve's differential coefficients. Our experiment results on simulated blurred images show that this method could give an acceptable estimate for the Gaussian blur parameter.

The rest of the paper is organized as follows. Section II describes the implementation of our identification method. Section III presents experimental results that illustrate the effectiveness of this approach, and the Section IV includes the concluding remarks.

II. Implementation of Parameter Identification

A. Search Space

Because the Gaussian PSF is characterized by a single parameter σ, the Gaussian blur identification is reduced to the estimation of the parameter σ.

Let

$$h^{(k)}(x,y) = h\left(x, y, \sigma^{(k)}\right) \tag{4}$$

where $\sigma^{(k)}$ is the kth element of the vector that contains the candidate parameters.

Let's make some constraints on the search space of all feasible parameter values. Let the "cameraman" image be degraded by Gaussian PSF of parameter $\sigma = 1$, and a Gaussian white noise at $\mathrm{BSNR} = 30\ \mathrm{dB}$ is added to the blurred image. Blurred signal-to-noise ratio (BSNR) is defined here as

$$\mathrm{BSNR} = 10\log_{10}\left(\frac{\sigma_b^2}{\sigma_n^2}\right)$$

where σ_b^2 is the variance of the blurred image. The blurred and noisy image is shown in Fig. 1(a). One can see from it that the Gaussian blur of parameter $\sigma = 1$ is very light. An alternative enhancement method may also obtain a satisfactory visual result as the restoration technology. The restoration result of Wiener filtering [see (10)] is shown in Fig. 1(b), and the enhancement result of unsharp masking technology [1], [7] is shown in Fig. 1(c).

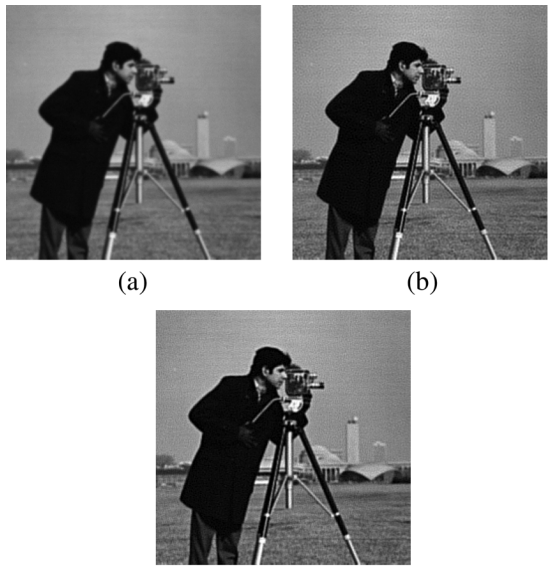

Fig. 1. (a) Gaussian blurred "cameraman" image of $\sigma = 1$ at $\mathrm{BSNR} = 30$ dB. (b) Restored image $\mathrm{ISNR} = 2.6651$ dB. (c) Enhanced image $\mathrm{ISNR} = 2.0691$ dB.

The improvement in signal-to-noise ratio (ISNR) of them are 2.6651 and 2.0691 dB, respectively. ISNR is defined as

$$\mathrm{ISNR} = 10\log_{10}\frac{\|f-g\|_2^2}{\|f-\hat{f}\|_2^2}.$$

One can see that almost identical visual results are obtained. So we can claim that when $\sigma \leq 1$, the deblurring result could be approximately obtained with enhancement technology.

Let's now consider $\sigma = 4$. The blurred and noisy result at $\mathrm{BSNR} = 30\ \mathrm{dB}$ of the "cameraman" image is shown in Fig. 2(a). One can see from it that the degradation caused by Gaussian blur of parameter $\sigma = 4$ is very severe. The restoration result of Wiener filtering (10) and the enhancement result of unsharp masking technology are shown in Fig. 2(b) and (c), respectively. The ISNR of them are 1.6134 and -0.0052 dB, respectively. It can be seen that in this case the enhancement technology result has no improvement. Though the restored image is better than the enhanced image, neither of them can give a satisfactory result. In this paper, we are concerned with the medium Gaussian blur that all feasible parameter σ values in the search space are in the domain $\sigma \in [1, 4]$. The search interval is set to 0.1. Then, the candidate parameters vector is

$$\begin{aligned}\mathbf{S} &= \{1 + (k-1)\times 0.1, k = 1, \cdots, 31\} \\ &= \{1, 1.1, 1.2, \cdots, 3.9, 4\}.\end{aligned} \tag{5}$$

B. Wiener Filter With Neumann Boundary Condition

In practice, the PSF h has a finite support and the observed image g is of finite size ($1 \leq x \leq M, 1 \leq y \leq N$). The task of image deblurring is to recover a finite section of the original image f in the domain ($1 \leq x \leq M, 1 \leq y \leq N$). From (1) one can see that g is not only determined by the values of the original image f in $[1:M, 1:N]$, but also affected by the values of f

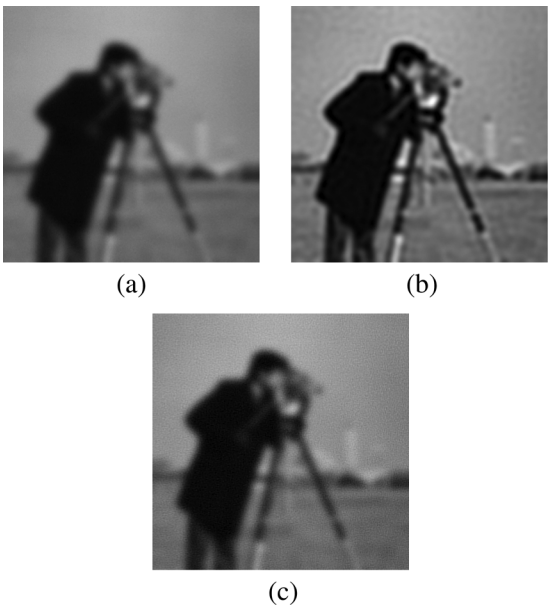

Fig. 2. (a) Gaussian blurred "cameraman" image of $\sigma = 4$ at $\mathrm{BSNR} = 30\,\mathrm{dB}$. (b) Restored image $\mathrm{ISNR} = 1.6134\,\mathrm{dB}$. (c) Enhanced image $\mathrm{ISNR} = -0.0052\,\mathrm{dB}$.

Fig. 3. (a) Gaussian blurred "cameraman" image of $\sigma = 3$ at $\mathrm{BSNR} = 30\,\mathrm{dB}$ (b) Restored image with periodic BC $\mathrm{ISNR} = 0.9589\,\mathrm{dB}$. (c) Restored image with Neumann BC $\mathrm{ISNR} = 1.7856\,\mathrm{dB}$.

out of the boundary. Support of h determines the interval out of the boundary. Thus in order to solve (1), some assumptions should be made as to the values of f outside $[1:M, 1:N]$. These assumptions are called boundary conditions (BC).

The form of the restored image's statistics depends on the type of restoration filter. The Wiener filter is chosen in our experiment for its fast implementation and acceptable result.

Let $\hat{F}(u,v)$ be the Wiener estimate of the original image in the frequency domain. Then

$$\hat{F}(u,v) = \frac{H^*(u,v)G(u,v)}{|H(u,v)|^2 + P_n(u,v)/P_f(u,v)} \tag{6}$$

where $H(u,v)$ is the PSF h in the frequency domain and is tested under the assumption that it is the true PSF, $G(u,v)$ is the blurred image in the frequency domain, and $P_f(u,v)$ and $P_n(u,v)$ are the power spectra of the original image and noise respectively. Because the power spectra of the original image and noise are sometimes hard to know, (6) is often simplified as

$$\hat{F}(u,v) = \frac{H^*(u,v)G(u,v)}{|H(u,v)|^2 + \tau} \tag{7}$$

where τ is the regularization parameter.

The estimate of the restored image is, thus, the inverse Discrete Fourier Transforms (DFT)

$$\begin{aligned}\hat{f}(x,y) &= \mathrm{IDFT}\left(\hat{F}(u,v)\right) \\ &= \sum_{u=1}^{M}\sum_{v=1}^{N} \hat{F}(u,v)\exp\{i2\pi(ux/M + vy/N)\}. \end{aligned} \tag{8}$$

In order to solve (8), DFT should be computed. Although the Fast Fourier Transforms (FFT) could be implemented in a very efficient way, the calculation of FFT takes it for granted that the boundary condition is periodic. So ringing effects would be unavoidable at the restored image's borders because natural image is seldom periodically structured.

In [16], Ng *et al.* used Neumann BC to reduce ringing effects and designed a fast algorithm to restore images. It assumes that the values of f outside the domain $[1:M, 1:N]$ is a reflection of the data inside. By using Neumann BC, the blurring matrix is a Toeplitz-plus-Hankel matrix in the 1–D case and a block Toeplitz-plus-Hankel matrix with Toeplitz-plus-Hankel blocks (BTHTHB) in the 2-D case. They showed that if the PSF is symmetric

$$h(x,y) = h(-x,y) = h(x,-y) = h(-x,-y) \quad \text{for all } x, y \tag{9}$$

the BTHTHB matrix could be diagonalized by the Discrete Cosine Transform (DCT-*IIE*) matrices. Then their inverses can be obtained by using Fast Cosine Transforms (FCT). This approach is computationally interesting since the FCT requires only real operations and is about twice as fast as the FFT [19], and this is also true in two dimensions.

Because the Gaussian PSF (3) we are concerned with in this paper satisfies the symmetric condition (9), our modified Wiener deconvolution with Neumann boundary condition is

$$\hat{F}_{dct}(u,v) = \frac{H_{dct}(u,v)G_{dct}(u,v)}{|H_{dct}(u,v)|^2 + \tau} \tag{10}$$

where the H_{dct} denotes the convolution matrix H's first column DCT result with Neumann BC and $G_{dct}(u,v)$ is the DCT of the degraded image.

Thus, the estimate of the restored image is the inverse DCT

$$\hat{f}(x,y) = \mathrm{IDCT}\left(\hat{F}_{dct}(u,v)\right). \tag{11}$$

The "cameraman" image is degraded by Gaussian blur of parameter $\sigma = 3$, and a Gaussian white noise is then added to it at $\mathrm{BSNR} = 30\,\mathrm{dB}$. The degraded image is shown in Fig. 3(a). The deblurring images of (7) and (10) with regularization parameter $\tau = 0.008$ are shown in Fig. 3(b) and (c), respectively. The ISNR of them are 0.9589 and 1.7856 dB, respectively. There

are severe ringing effects in Fig. 3(b), and (c) is more suitable for error analysis.

C. Analysis of the Restored Image

Once the restoration method has been chosen and the set of candidate parameters has been constructed, it remains to select the best estimate from the set $\mathbf{S}$.

Let the restored image be expressed as $\hat{f}^{(k)}(x,y)$, which is the deblurring result with (10) that has the kth element of candidate parameters set $h^{(k)}(x,y)$ as the PSF.

Let $\mathrm{SDN}^{(k)}$ be the L1 norm of $\hat{f}^{(k)}(x,y)$'s second derivatives

$$\mathrm{SDN}^{(k)} = \left\| \nabla^2 \hat{f}^{(k)} \right\|_1 = \left\| \hat{f}^{(k)}_{xx} + \hat{f}^{(k)}_{yy} \right\|_1 \tag{12}$$

where ∇^2 is the Laplacian operator, and is defined as $\nabla^2 I = (\partial^2 I/\partial x^2) + (\partial^2 I/\partial y^2)$. In our experiment, the discrete implementation of the two-dimensional Laplacian operator is set as

$$\nabla^2 f = f(x+1,y) + f(x-1,y) + f(x,y+1) + f(x,y-1) - 4f(x,y). \tag{13}$$

For a blurred image $g(x,y)$, all of the $\mathrm{SDN}^{(k)}$ corresponding to each candidate parameter in the search set $\mathbf{S}$ could form into a curve. We term it restored image Laplacian L1 norm curve (L1C) of the degraded image.

$$L1C(k) = \mathrm{SDN}^{(k)}. \tag{14}$$

The differential coefficients of this curve are called as $DL1C$

$$DL1C(k) = L1C(k+1) - L1C(k). \tag{15}$$

Let the "cameraman" image be blurred by one of the PSF $h^{(k)}(x,y)$ and a Gaussian white noise is added to it at $\mathrm{BSNR} = 40$ dB. The blurred image is restored by (10) with regularization parameter $\tau = 0.004$ for each candidate parameter in the search set under the assumption that it is the true PSF. Therefore, we can get the L1C and DL1C of the blurred image. The degraded images that are blurred by Gaussian PSFs of parameters $\sigma = 1.5$, $\sigma = 2.5$, and $\sigma = 3.5$ are shown in Fig. 4. Their corresponding L1C and DL1C are shown in Fig. 5. We normalize them in the plot, because it does not change the curve's shape. The location of the true parameter is plotted with a vertical line, the minimum point of the L1C and the maximum point of the DL1C are marked with '$*$'. One can see from Fig. 5(a) that there is a weak relationship between the minimum point of L1C and the true parameter. An interesting phenomenon could be observed from Fig. 5(b) that the maximum point of DL1C is always close to the correct value. So the abscissa $x_{\max}$ of the maximum point of DL1C could be a robust estimate of the Gaussian blur parameter. This is also true for other true parameter σ values, which can be seen in Table I. One can see from Table I that the maximum deviation between $x_{\max}$ and the true parameter is 0.3, and most of the deviation is within 0.1. This is a commonly receivable result.

Let's consider the behavior of L2 norm of the restored image's second derivatives $\|\nabla^2 \hat{f}^{(k)}\|_2$ and its differential coefficients (correspondingly, we call them L2C and DL2C). The L2C and DL2C corresponding to Fig. 4 are shown in Fig. 6.

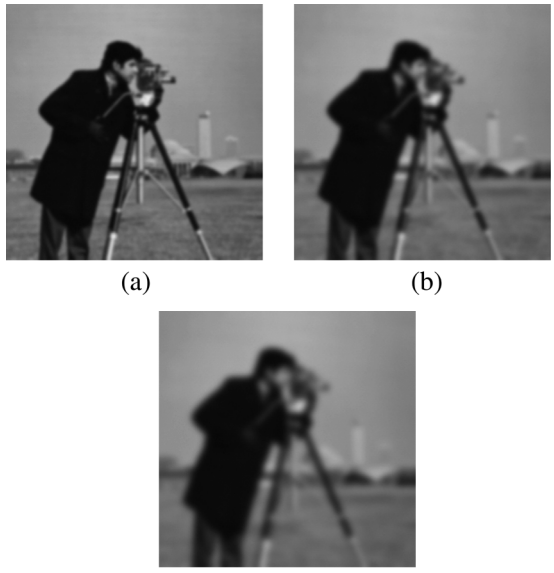

(a) (b) (c)

Fig. 4. (a) Gaussian blurred "cameraman" image of $\sigma = 1.5$ at $\mathrm{BSNR} = 40$ dB. (b) Gaussian blurred "cameraman" image of $\sigma = 2.5$ at $\mathrm{BSNR} = 40$ dB. (c) Gaussian blurred "cameraman" image of $\sigma = 3.5$ at $\mathrm{BSNR} = 40$ dB.

One can see by comparing it to Fig. 5 that the maximum point of DL2C is not as robust as the DL1C. It is also true for other σ values, which can be seen from Table I. Therefore, the L1 norm is preferred in our experiment.

It has been shown in Section II-B that the Neumann BC is better than the periodic BC for error analysis. Let's see the numerical comparison between them. Plots of L1C and DL1C of Fig. 4 with periodic BC (i.e., deblurring Fig. 4 with (7)) are shown in Fig. 7. It can be seen that the curves in Fig. 7 are not as smooth as those in Fig. 5 and Fig. 6. From Table I, one can see that the DL1C with periodic BC is not as robust as the DL1C with Neumann BC. The reason is that the errors caused by the ringing effects at the restored image's borders have a significant impact on the L1 norm.

The estimated values from the DL1C with Neumann BC, DL2C with Neumann BC, and the DL1C with periodic BC to each of the true parameters are shown in Table I. The plot of each is shown in Fig. 8. In it, the true parameter value is plotted with the diagonal line. One can see that the DL1C with Neumann BC performs the best.

III. Experiments

A. Test Image Set

We test this method on an image set which includes 15 standard images. The image set is depicted in Fig. 9. We test these 15 images at different BSNR levels of 30, 40, and 50 dB. Comparison is taken among these metrics: L1C, DL1C, L2C, and DL2C with Neumann BC and periodic BC, respectively. We observe that in all these cases the Neumann BC outperforms the periodic BC. Among the four Neumann BC metrics, DL1C and DL2C outperform L1C and L2C. Only in eight cases, the DL2C with Neumann BC is a litter better than the DL1C with Neumann BC. Another interesting observation is that, among these

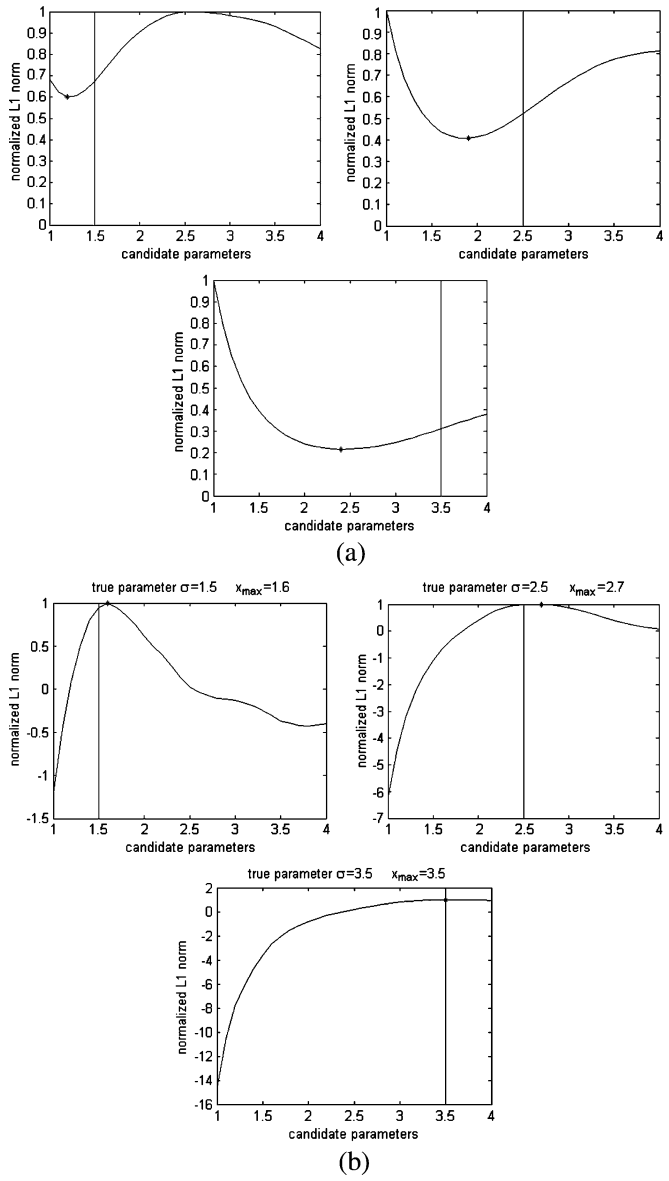

Fig. 5. L1C and DL1C of parameters $\sigma = 1.5$, $\sigma = 2.5$, and $\sigma = 3.5$. Location of the true parameter is plotted with a vertical line. The minimum point of L1C and the maximum point of DL1C are marked with $*$. (a) L1C. (b) DL1C.

eight cases, five cases are at $\mathrm{BSNR} = 30\ \mathrm{dB}$, two cases are at $\mathrm{BSNR} = 40\ \mathrm{dB}$, and only one case is at $\mathrm{BSNR} = 50\ \mathrm{dB}$. This means that DL1C performs much better than DL2C at higher SNR. In most cases the DL1C is more robust than DL2C as seen in Fig. 8. So the DL1C with Neumann BC is chosen as the metric we use to estimate parameter values.

The DL1C maximization method is also compared with kurtosis minimization (KM) [15] in every case. Parts of the results are shown in the following. The results of image "cameraman" are shown in Fig. 10. One can see, our method outperforms KM at BSNR $= 40$, 50 dB. Though at $\mathrm{BSNR} = 30\ \mathrm{dB}$ parts of the KM's results are a little better than our method, it fails when the $\sigma > 3.2$. The comparison result of another standard image Lena is shown in Fig. 11. One can see that our method can obtain a better result than KM at all the three noise levels. The result of image "bridge" is shown in Fig. 12. It can be seen that in these cases the KM method fails, whereas our method can still get a reliable result. The other results, which are not shown here as space is limited, also support that at average our method outperforms KM.

TABLE I
$x_{\max}$ OF DL1C WITH NEUMANN BC, DL2C WITH NEUMANN BC, AND DL1C WITH PERIODIC BC. (ABBREVIATION: TRUE PARAMETER (TP); AE (Absolute error $= \mathrm{abs}(x_{\max} - TP)$); DL1C WITH NEUMANN BC (1N); DL2C WITH NEUMANN BC (2N); DL1C WITH PERIODIC BC (1P);)

TP	**1.0**	**1.1**	**1.2**	**1.3**	**1.4**	**1.5**	**1.6**
AE(1N)	0.1	0.1	0.1	0.1	0.1	0.1	0.1
AE(2N)	0.1	0.1	0.1	0.1	0.1	0.1	0.1
AE(1P)	0.1	0.2	0.2	0.1	0	0.1	0.2
TP	**1.7**	**1.8**	**1.9**	**2.0**	**2.1**	**2.2**	**2.3**
AE(1N)	0.1	0.1	0.1	0.1	0.1	0.1	0.1
AE(2N)	0.2	0.2	0.2	0.2	0.2	0.3	0.4
AE(1P)	0.2	0.1	0	0.1	0	0.1	0.2
TP	**2.4**	**2.5**	**2.6**	**2.7**	**2.8**	**2.9**	**3.0**
AE(1N)	0	0.2	0.1	0.1	0.1	0	0
AE(2N)	0.5	0.4	0.3	0.3	0.4	0.5	0.5
AE(1P)	0.2	0.1	0	0	0.1	0	0.1
TP	**3.1**	**3.2**	**3.3**	**3.4**	**3.5**	**3.6**	**3.7**
AE(1N)	0	0.1	0	0	0	0	0.3
AE(2N)	0.7	0.8	0.7	0.6	0.5	0.4	0.3
AE(1P)	0.2	0.2	0.1	0	0.1	0.1	0
TP	**3.8**	**3.9**	**4.0**				
AE(1N)	0.2	0.1	0				
AE(2N)	0.2	0.1	0				
AE(1P)	0.1	0.2	0.3				

B. Mean Estimated Value

In our experiment, we have found that, although the estimated values of all test images are a little different from each other, they are all within a short distance to the true parameter. The estimated values corresponding to each true parameter of all test images are shown in Fig. 13, at the noise level of $\mathrm{BSNR} = 40\ \mathrm{dB}$. The mean values of them are plotted with a bold line. For each true parameter, the mean, the maximum, and the minimum estimated values are shown in Table II. We have found in our experiment that the distribution of the estimated values of each true parameter can be approximated as a

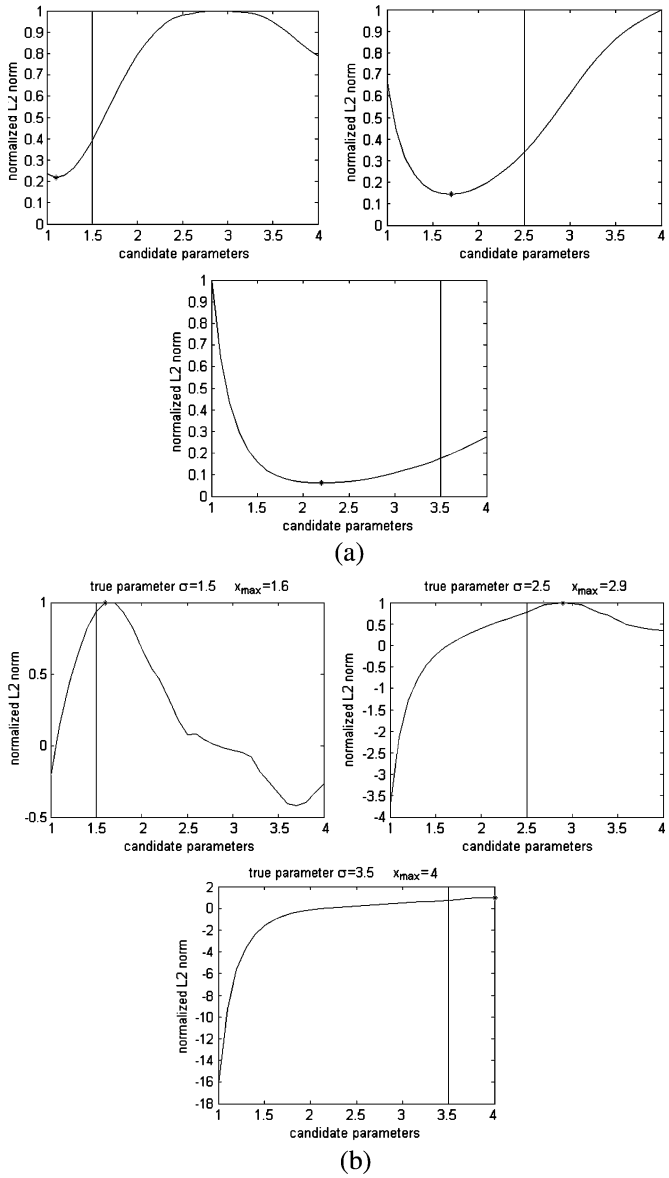

Fig. 6. L2C and DL2C of parameters $\sigma = 1.5$, $\sigma = 2.5$, and $\sigma = 3.5$. Location of the true parameter is plotted with a vertical line. The minimum point of L2C and the maximum point of DL2C are marked with $*$. (a) L2C. (b) DL2C.

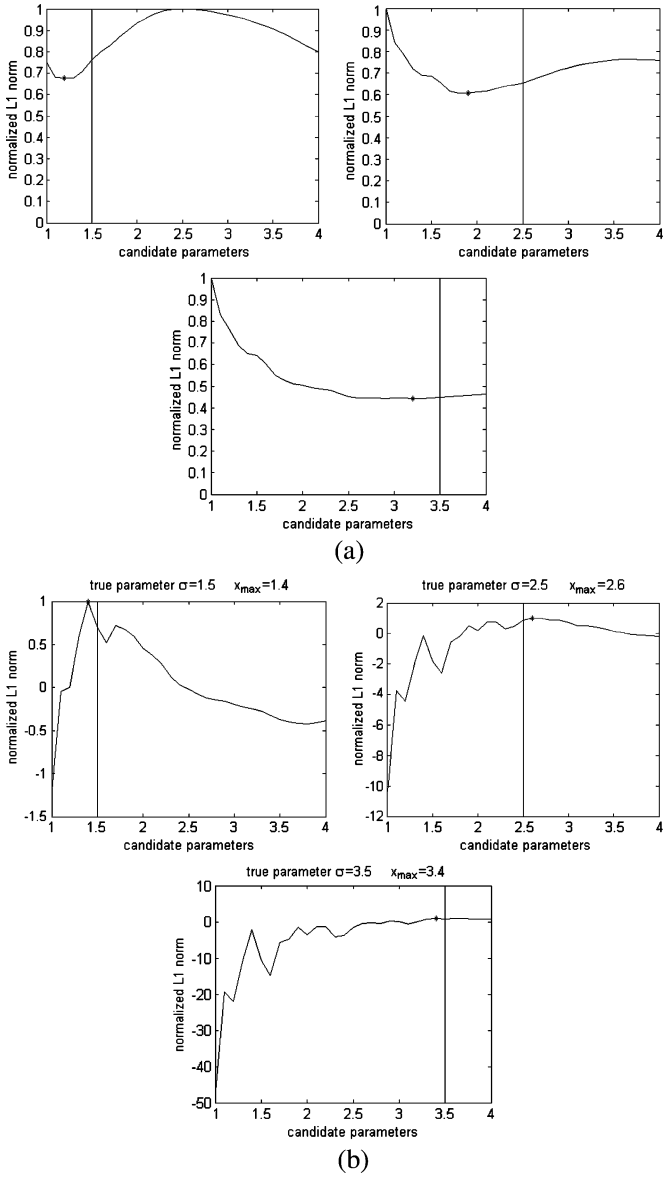

Fig. 7. L1C and DL1C with periodic BC of parameters $\sigma = 1.5$, $\sigma = 2.5$, and $\sigma = 3.5$. Location of the true parameter is plotted with a vertical line. The minimum point of L1C and the maximum point of DL1C are marked with $*$. (a) L1C. (b) DL1C.

Gaussian distribution. A quadratic polynomial curve fitting is done to fit the mean estimated values. The fitting result is

$$mv = -0.0137 \times tv^2 + 1.0059 \times tv + 0.0737 \; (mv > 0, 4 \geq tv \geq 1) \tag{16}$$

where mv is the mean estimated value and tv is the true parameter value.

We have tested this identification method at different noise levels. The estimated curves and their mean values, at the noise level of BSNR $= 50$ dB and BSNR $= 30$ dB, are shown in Figs. 14 and 15, respectively. Quadratic polynomial curve fittings to their mean estimated values are

$$mv = -0.0097 \times tv^2 + 1.0278 \times tv - 0.0133 \; (mv > 0, 4 \geq tv \geq 1) \tag{17}$$

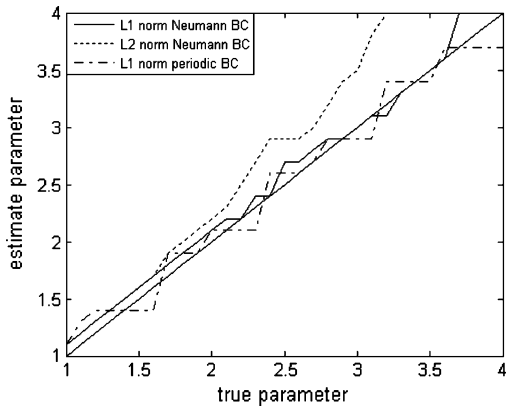

Fig. 8. Estimated values of the DL1C with Neumann BC, DL2C with Neumann BC, and the DL1C with periodic BC.

Fig. 9. Test standard image set.

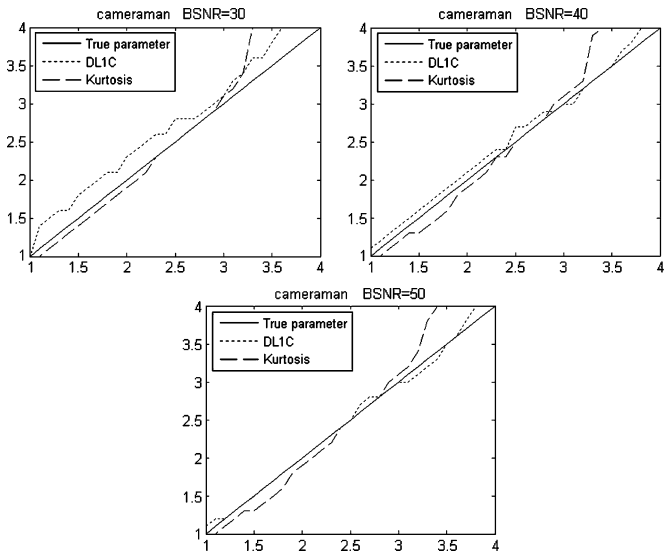

Fig. 10. Compare with kurtosis minimization ("cameraman" image).

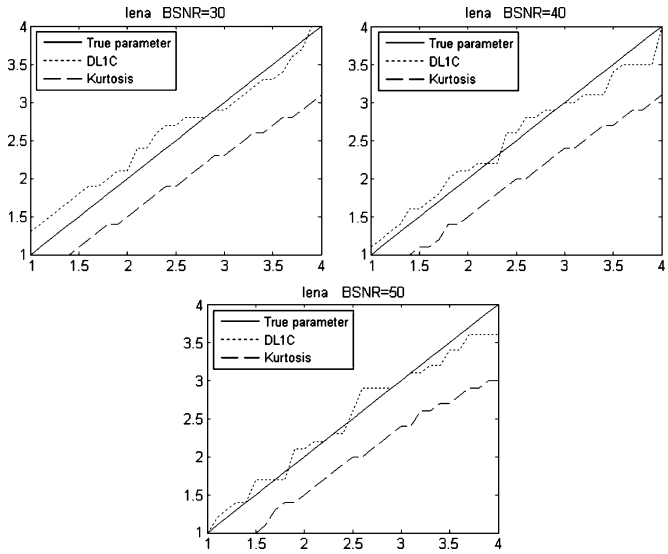

Fig. 11. Compare with kurtosis minimization ("Lena" image).

and

$$mv = -0.0130 \times tv^2 + 0.9334 \times tv + 0.3227 \ (mv > 0, 4 \geq tv \geq 1). \tag{18}$$

One can see from the three mean estimated values curves at different noise level that the method we proposed is likely to obtain a lower estimate at noise level BSNR $= 30$ dB and is likely to obtain a higher estimate at noise level like BSNR $=$ 50 dB.

One can see, in order to get an accurate estimate, the BSNR should be known first. Fortunately, there are several practical methods proposed in the literature to estimate it reliably from the degraded image [9], [17], [18]. Even if one could not get an accurate estimate of the BSNR, from our experience of this method, $x_{\max}$ is still a reliable estimate.

The identification procedure of our method can be concluded as: for a degraded image, first estimate BSNR from the degraded image and compute the corresponding best regularization parameter with (19). Second, compute DL1C of the degraded image in the search space $\mathbf{S}$. Third, exhaustively search for the abscissa $x_{\max}$ of its maximum point. Fourth, choose the corresponding empirical equation. Finally, let $mv = x_{\max}$ (it is the result of maximum likelihood (ML) principle if we assume that the Gaussian probability distributions of the estimated values of all true parameters are the same), compute the corresponding tv with the chosen equation and tv is the best estimate of our method.

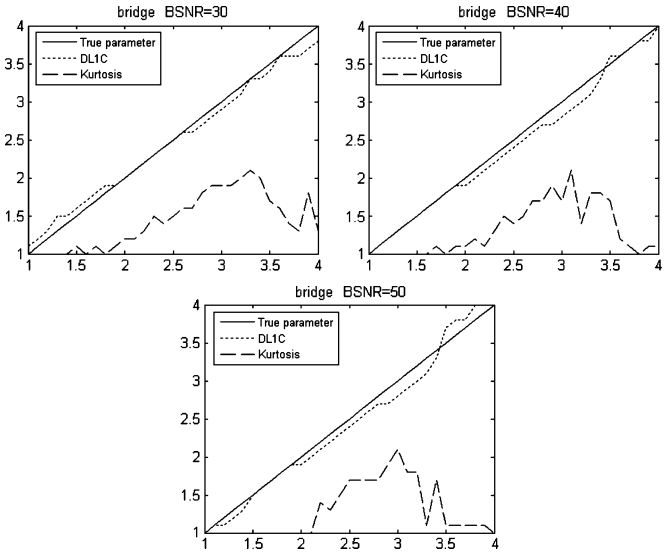

Fig. 12. Compare with kurtosis minimization ("bridge" image).

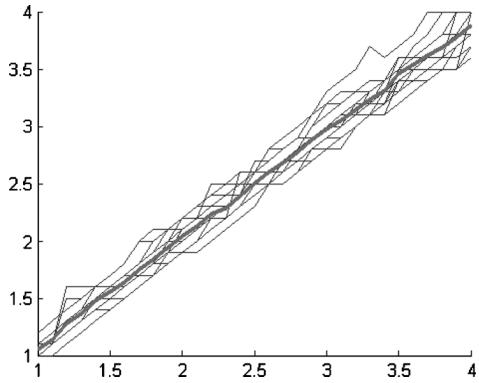

Fig. 13. Mean of the estimated values at $\mathrm{BSNR} = 40$ dB.

C. Regularization Parameter τ

The regularization parameter τ plays an important role in the deblurring method. It controls the tradeoff between fidelity to the data and smoothness of the solution. There are two automatic techniques to estimate the regularization parameter, the Generalized cross-validation (GCV) [6] and the L-curve [8]. However, both of them are computationally expensive and the results are sometimes not satisfactory.

In our experiment, we manually test some τ values in the set

$$\tau = [0.05, 0.025, 0.01, 0.009, 0.008, 0.007, 0.006, 0.005, 0.004, 0.003, 0.002, 0.001]$$

for the test image set. The mean estimate values of each τ are computed. Among these curves, we choose the τ value whose mean estimate value curve is the closest to the diagonal line. Comparison is taken at different noise levels of BSNR $= 20, 30, 40, 50, 60, 80, 100$ dB. Among them it is found that $\tau = 0.008$ performs the best at noise level BSNR $= 30$ dB, $\tau = 0.004$ performs the best at noise level BSNR $= 40$ dB, and $\tau = 0.003$ performs the best at noise level BSNR ≥ 50 dB. Estimation results are shown in Fig. 16.[1] One can see, deblurring with a small τ value often leads to a lower estimate than the true parameter. Meanwhile, a large τ leads to a higher estimate. The experiment results of other BSNR noise levels show that the best regularization parameters are all 0.003 when the BSNR is higher than 50 dB. The results also show that the best τ is 0.025 when the BSNR is 20 dB, but some of the estimate errors may be larger than 0.5, which is not a reliable estimate.

From our experiment results, we suggest choosing the regularization parameter τ with Gaussian interpolation (19).

[1]Only parts of the regularization parameters are plotted for distinguishable showing.

TABLE II
MEAN ESTIMATE, MAXIMUM ESTIMATE, AND MINIMUM ESTIMATE OF EACH TRUE PARAMETER

True Parameter	**1.0**	**1.1**	**1.2**	**1.3**	**1.4**	**1.5**	**1.6**
Mean estimate	1.05	1.13	1.28	1.37	1.48	1.55	1.64
Max estimate	1.2	1.3	1.6	1.6	1.6	1.7	1.8
Min estimate	1.0	1.0	1.1	1.2	1.3	1.4	1.5
True Parameter	**1.7**	**1.8**	**1.9**	**2.0**	**2.1**	**2.2**	**2.3**
Mean estimate	1.75	1.84	1.95	2.04	2.13	2.23	2.29
Max estimate	2.0	2.1	2.1	2.2	2.3	2.5	2.5
Min estimate	1.6	1.7	1.8	1.9	1.9	2.0	2.1
True Parameter	**2.4**	**2.5**	**2.6**	**2.7**	**2.8**	**2.9**	**3.0**
Mean estimate	2.39	2.51	2.6	2.68	2.77	2.88	2.98
Max estimate	2.6	2.7	2.8	2.9	3.0	3.1	3.3
Min estimate	2.2	2.3	2.5	2.5	2.6	2.7	2.8
True Parameter	**3.1**	**3.2**	**3.3**	**3.4**	**3.5**	**3.6**	**3.7**
Mean estimate	3.05	3.15	3.23	3.31	3.46	3.54	3.62
Max estimate	3.4	3.5	3.7	3.6	3.7	3.8	4.0
Min estimate	2.8	3.0	3.1	3.1	3.2	3.3	3.4
True Parameter	**3.8**	**3.9**	**4.0**				
Mean estimate	3.69	3.77	3.88				
Max estimate	4.0	4.0	4.0				
Min estimate	3.5	3.5	3.6				

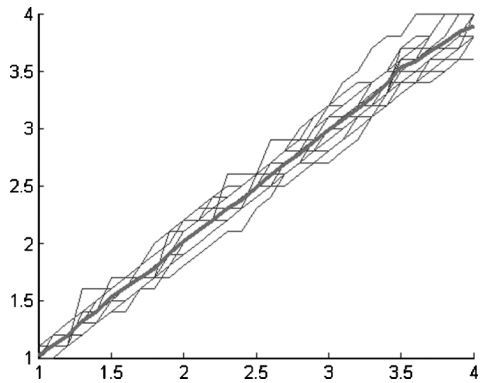

Fig. 14. Mean of the estimated values at $\mathrm{BSNR} = 50$ dB.

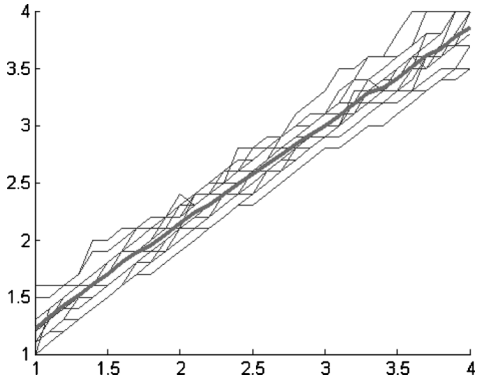

Fig. 15. Mean of the estimated values at $\mathrm{BSNR} = 30$ dB.

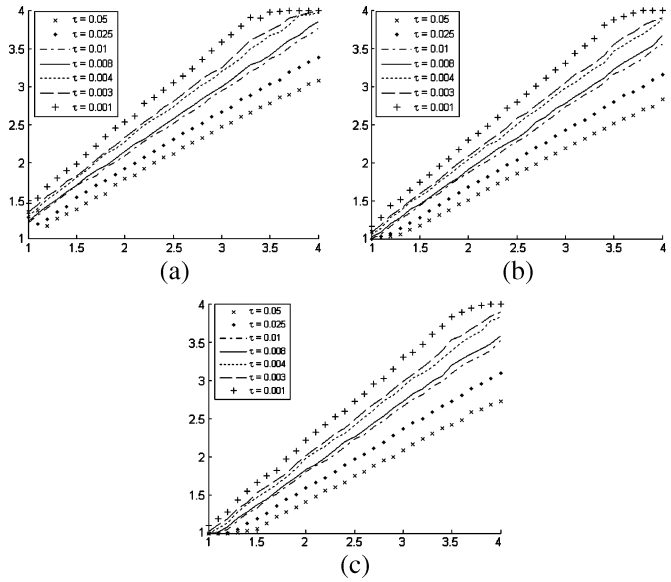

Fig. 16. Estimated values with different regularization parameter τ. (a) $\mathrm{BSNR} = 30$ dB. (b) $\mathrm{BSNR} = 40$ dB. (c) $\mathrm{BSNR} = 50$ dB.

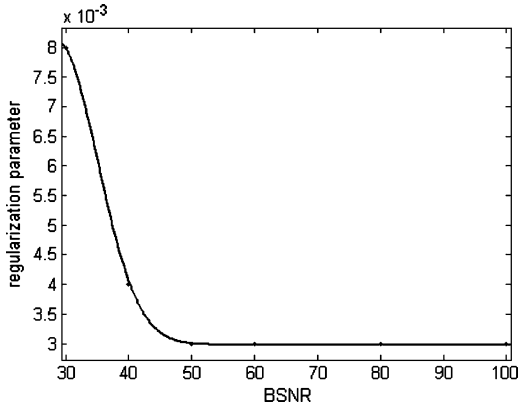

Fig. 17. Regularization parameter Gaussian interpolation curve.

Though other interpolation methods could be used, the differences between them may be very small. The interpolation curve is plotted in Fig. 17.

$$y = 0.005128 * e^{\left(-((x-28.56)/9.171)^2\right)} + 0.002982 * e^{\left(-((x-100)/2794000)^2\right)} \quad (x \geq 30). \quad (19)$$

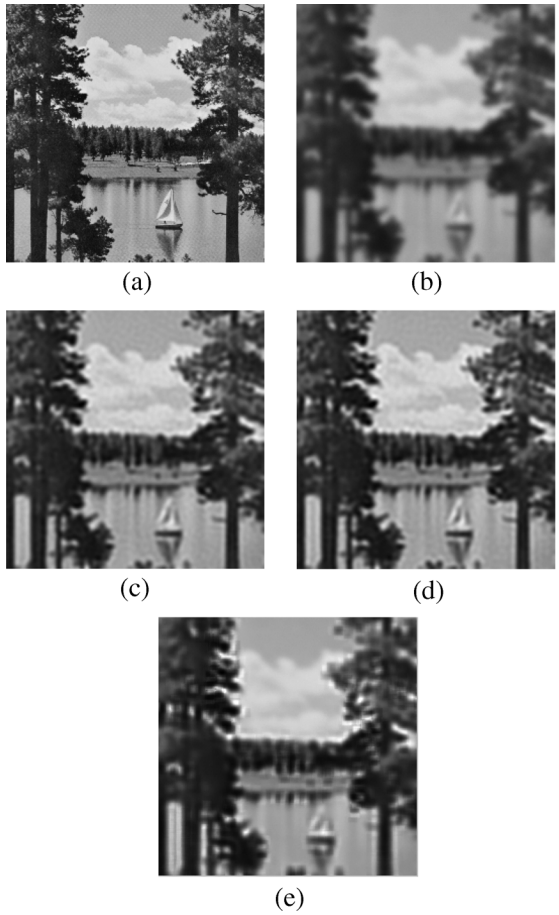

Fig. 18. (a) Original "Lake" image. (b) Gaussian blurred image of $\sigma = 2.7$ at $\mathrm{BSNR} = 40$ dB. (c) Restored image by true value $\sigma = 2.7$; $\mathrm{ISNR} = 2.1050$ dB. (d) Restored image by estimated value $\sigma = 2.8185$, $\mathrm{ISNR} = 2.0781$ dB. (e) Restored image by the MATLAB function "deconvblind" with initial PSF size of (9,9), $\mathrm{ISNR} = 0.8860$ dB.

D. Deblurring With Parameter Identification

Another standard image "lake" in Fig. 18(a), which is not included in the image set, is used to test the validity of our method. It is degraded by Gaussian PSF of $\sigma = 2.7$, and a white Gaussian noise is added to the blurred image at $\mathrm{BSNR} = 40$ dB. The degraded image is shown in Fig. 18(b). The DL1C of the blurred and noisy image is shown in Fig. 19. The maximum point's abscissa $x_{\max}$ of it is 2.8. The BSNR is estimated by the method proposed in [9] and it is $\mathrm{BSNR} = 40.0763$ dB ≈ 40 dB. From (16), we can get the estimated parameter by the proposed method, which is 2.8185. The restored image by the estimated value $\sigma = 2.8185$ is shown in Fig. 18(d). For comparison, the restored image by the true value $\sigma = 2.7$ is also shown in Fig. 18(c). Almost identical visual results are obtained. The ISNR of Fig. 18(c) and (d) are 2.1050 and 2.0781 dB, respectively. There are small differences between them.

Let the "lake" image be blurred by another Gaussian PSF of parameter $\sigma = 1.9$, and white Gaussian noise is added to the blurred image at noise level $\mathrm{BSNR} = 35$ dB. The estimated BSNR is 38.0667 dB and the best regularization parameter with (19) is 0.0047. The maximum point's abscissa $x_{\max}$ of DL1C is 2, which is shown in Fig. 21. Although we could also compute the mean estimated value curve at $\mathrm{BSNR} = 38$ dB like at the

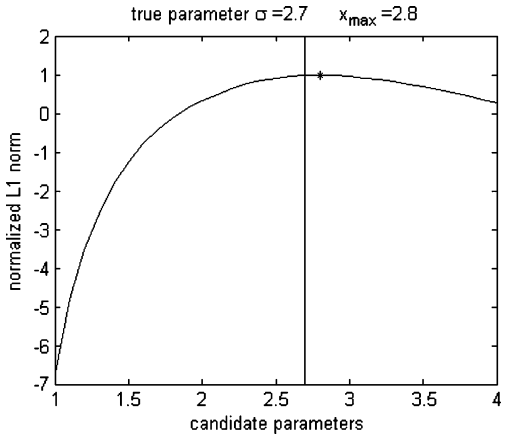

Fig. 19. DL1C of Fig. 18(b).

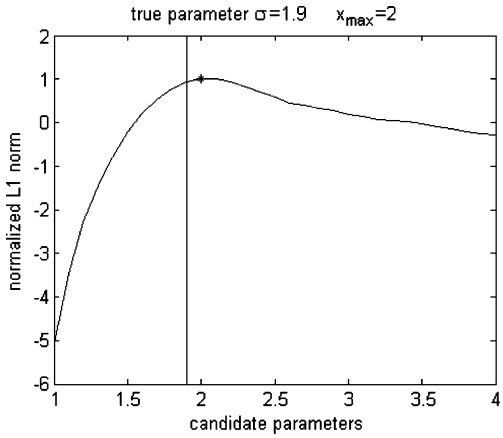

Fig. 21. DL1C of Fig. 20(a).

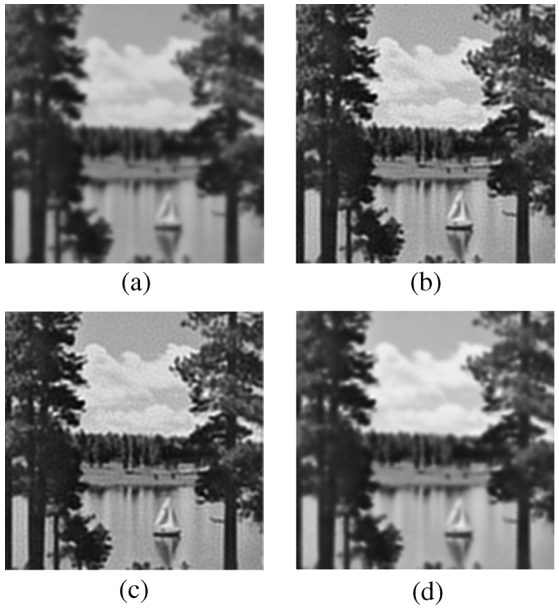

Fig. 20. (a) Gaussian blurred image of $\sigma = 1.9$ at BSNR $= 35$ dB. (b) Restored image by true value $\sigma = 1.9$, ISNR $= 2.8034$ dB. (c) Restored image by estimated value $\sigma = 1.9513$, ISNR $= 2.8017$ dB. (d) Restored image by the MATLAB function "deconvblind" with initial PSF size of (5,5), ISNR $= 0.9255$ dB.

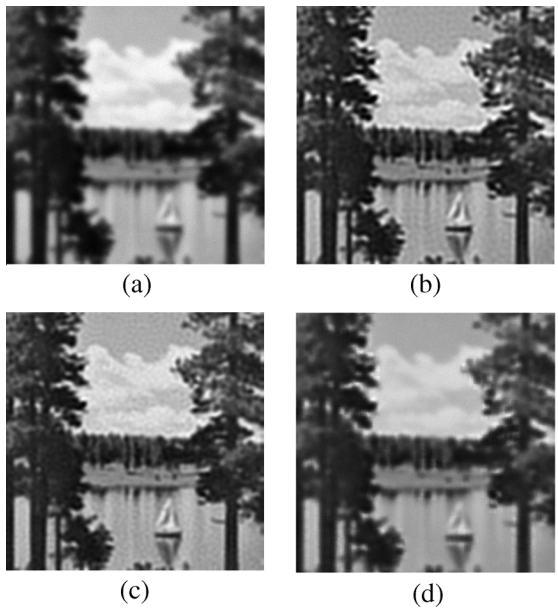

Fig. 22. (a) Blurred image by a nearly Gaussian PSF, which is combined by a Gaussian PSF of $\sigma = 2$, a defocus PSF of radius $r = 2$ and a horizontal motion PSF of length 1.5, at noise level BSNR $= 30$ dB. (b) Restored image by estimated Gaussian PSF of $\sigma = 2.5797$, ISNR $= 2.1288$ dB; (c) Restored image by true PSF ISNR $= 2.4283$ dB. (d) Restored image by "deconvblind" with initial PSF size of (7,7), ISNR $= 0.9902$ dB.

noise levels BSNR $= 30$, 40, 50 dB, an alternate interpolation method is used here to estimate the parameter. From (18), (16), and (17), we can compute the estimated values at these three noise levels BSNR $= 30$, 40, 50 dB, which are 1.8444, 1.9677, and 1.9965, respectively. The interpolation value at 38.0667 dB is 1.9513 with the quadric polynomial interpolation method. The restored images by the true value $\sigma = 1.9$ and by the estimated value $\sigma = 1.9513$ are shown in Fig. 20(b) and (c). Their ISNR are 2.8034 and 2.8017 dB, respectively.

We have also tested the performance of our method on nearly Gaussian PSF. Let the "lake" image be blurred by a nearly Gaussian PSF, which is combined by a Gaussian PSF of $\sigma = 2$, a defocus PSF of radius $r = 2$ and a horizontal motion PSF of length 1.5, at noise level BSNR $= 30$ dB. The blurred image is shown in Fig. 22(a), and its DL1C is shown in Fig. 23. The estimated σ by our method is 2.5797. The restored image by our estimated Gaussian PSF is shown in Fig. 22(b), and the restored image with the true nearly Gaussian PSF is shown in Fig. 22(c). Visually, they are very similar. Their ISNR are 2.1288 and 2.4283 dB, respectively. It can be seen that our method can estimate a Gaussian PSF to approximate the true nearly Gaussian PSF, and achieve a visually similar restoration result.

For comparison, the MATLAB function "deconvblind" is tested.[2] The restoration result of Fig. 18(b) by function "deconvblind" with initial PSF size of (9,9) is shown in Fig. 18(e). It can be seen that it is not a good result. The restoration result of Fig. 20(a) by "deconvblind" with initial PSF size of (5,5) is shown in Fig. 22(d). This result is also not good. The restoration result of Fig. 22(a) by "deconvblind" function with initial PSF

[2]The MATLAB function "deconvblind" is sensitive to the initial PSF size. We manually test the initial PSF size from (3,3) to (17,17), and only the best one among them is shown here as space is limited.

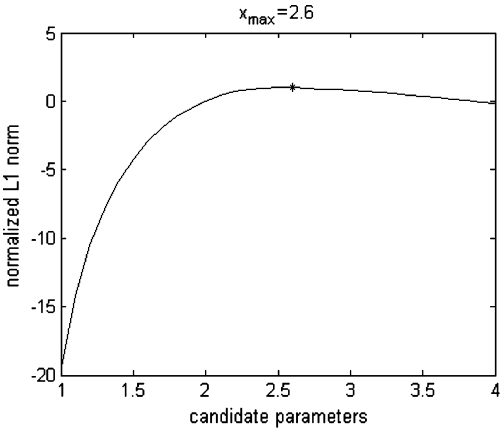

Fig. 23. DL1C of Fig. 22(a).

size of (7,7) is shown in Fig. 22(d), and its ISNR is 0.9902 dB. One can see that Fig. 22(d) is not a satisfactory result, and our method with an approximated Gaussian PSF estimation performs better than it.

From our experiment results, it is believed that our method can be applied to restore the images that are degraded by a Gaussian or nearly Gaussian PSF. In this condition, our method can estimate a Gaussian function to approximate the true nearly Gaussian PSF and achieve an acceptable restoration result. The experiment results also prove that our method is more effective than the blind deconvolution function "deconvblind" offered by MATLAB.

E. Computational Complexity

The identification method of the medium Gaussian blur parameter as described above chooses a best estimate from search space $\mathbf{S}$, which includes 31 candidate parameters. Realization of it requires 31 deblurring operations, i.e. the simplified Wiener filter with Neumann BC (10). Implementation of (10) is very fast because it requires only $O(N^2 log(N))$ real operations. Computation of the discrete Laplacian operator needs only four addition operations and one multiplication operation to compute each output pixel, so the computation load of DL1C is $O(N^2)$. The computation load of searching for the abscissa $x_{\max}$ and solving the empirical quadratic polynomial equation like (16) is minor.

IV. Conclusion

An empirical identification method of the medium Gaussian blur parameter for image deblurring is presented. This method chooses the best estimate from a set of candidate parameters. It first estimates the BSNR from the degraded image and computes the corresponding best regularization parameter. Next, it computes the L1 norm of the restored image's second derivatives for all candidates under the assumption that it is the true PSF, and then finds the maximum point's abscissa $x_{\max}$ of the DL1C. Finally, it chooses the corresponding empirical equation and computes the estimate of the true parameter. Experimental results presented in this paper demonstrate that this method performs well for medium Gaussian/nearly Gaussian blur.

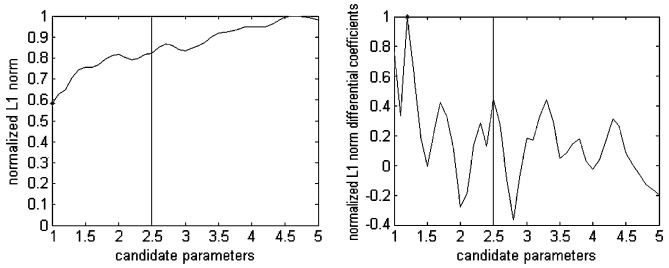

Fig. 24. L1C and DL1C of the defocus blurred and noisy "cameraman" image of defocus radius parameter 2.5 at noise level BSNR $= 40$ dB.

Although it seems that our blur parameter identification method is model-independent, and can be extended to the parameter identification of defocus blur and motion blur models, unfortunately, from our experiment results, this method does not perform well for these two blur models. The L1C and DL1C of the defocus blurred and noisy "cameraman" image with blur radius parameter 2.5 at noise level BSNR $= 40$ dB are drawn in Fig. 24. No obvious relationship can be found between the maximum point and the true parameter value. It is almost certainly due to the intrinsic differences among various blur models, which still requires more investigation.

Acknowledgment

The authors would like to thank the anonymous referees for their helpful comments.

References

[1] T. Acharya and A. K. Ray, *Image Processing Principles and Applications*. Hoboken, NJ: Wiley, 2005.
[2] H. Andrew and B. Hunt, *Digital Image Restoration*. Englewood Cliffs, NJ: Prentice-Hall, 1977.
[3] M. R. Banham and A. K. Katsaggelos, "Digital image restoration," *IEEE Signal Process. Mag.*, vol. 14, no. 2, pp. 24–41, Mar. 1997.
[4] M. M. Chang, A. M. Tekalp, and A. T. Erdem, "Blur identification using the bispectrum," *IEEE Trans. Signal Process.*, vol. 39, no. 10, pp. 2323–2325, Oct. 1991.
[5] D. B. Gennery, "Determination of optical transfer function by inspection of frequency-domain plot," *J. Opt. Soc. Amer.*, vol. 63, no. 12, pp. 1571–1577, Dec. 1973.
[6] G. Golub, M. Heath, and G. Wahba, "Generalized cross-validation as a method for choosing a good ridge parameter," *Technometr.*, vol. 21, no. 2, pp. 215–223, May 1979.
[7] R. Gonzalez and R. Woods, *Digital Image Processing (Second Edition)*. Upper Saddle River, NJ: Prentice-Hall, 2002.
[8] P. C. Hansen and D. P. O'Leary, "The use of the L-curve in the regularization of discrete ill-posed problems," *SIAM J. Sci. Comput.*, vol. 14, no. 6, pp. 1487–1503, Nov. 1993.
[9] J. Immerkaer, "Fast noise variance estimation," *Comp. Vision Image Understand.*, vol. 64, no. 2, pp. 300–302, Sep. 1996.
[10] A. K. Katsaggelos, *Digital Image Restoration*. New York: Springer-Verlag, 1991.
[11] R. L. Lagendijk, J. Biemond, and D. E. Boekee, "Regularized iterative image restoration with ringing reduction," *IEEE Trans. Acoust., Speech, Signal Process.*, vol. 36, no. 12, pp. 1874–1888, Dec. 1988.
[12] R. L. Lagendijk, J. Biemond, and D. E. Boekee, "Identification and restoration of noisy blurred images using the expectation-maximization algorithm," *IEEE Trans. Acoust., Speech, Signal Process.*, vol. 38, no. 7, pp. 1180–1191, Jul. 1990.
[13] R. L. Lagendijk, A. M. Tekalp, and J. Biemond, "Maximum likelihood image and blur identification: A unifying approach," *Opt. Eng.*, vol. 29, no. 5, pp. 422–435, May 1990.

[14] D. Li, R. M. Mersereau, and S. Simske, "Blur identification based on kurtosis minimization," *IEEE Proc. Int. Conf. Image Process.*, vol. 1, pp. 905–908, Sep. 2005.
[15] D. Li, "Restoration of atmospheric turbulence degraded video using kurtosis minimization and motion compensation," Ph.D. dissertation, Georgia Inst. Technol., Atlanta, 2007.
[16] M. K. Ng, R. H. Chan, and W. C. Tang, "A fast algorithm for deblurring models with neumann boundary conditions," *SIAM J. Sci. Comput.*, vol. 21, no. 3, pp. 851–866, May 1999.
[17] S. I. Olsen, "Estimation of noise in images: An evaluation," *CVGIP: Graph. Models Image Process.*, vol. 55, no. 4, pp. 319–323, Jul. 1993.
[18] K. Rank, M. Lendl, and R. Unbehauen, "Estimation of image noise variance," *IEE Proc. Vision, Image, Signal Process.*, vol. 146, no. 2, pp. 80–84, Apr. 1999.
[19] K. Rao and P. Yip, *Discrete Cosine Transform: Algorithms, Advantages, Applications*. New York: Academic, 1990.
[20] S. J. Reeves and R. M. Mersereau, "Blur identification by the method of generalized cross-validation," *IEEE Trans. Image Process.*, vol. 1, no. 3, pp. 301–311, Jul. 1992.
[21] A. E. Savakis and H. J. Trussell, "Blur identification by residual spectral matching," *IEEE Trans. Image Process.*, vol. 2, no. 2, pp. 141–151, Apr. 1993.

Fen Chen (M'08) received the B.S. and M.S. degrees in 2000 and 2002, respectively, from the Wuhan University, Wuhan, China, and the Ph.D. degree from the Institute of Remote Sensing Applications, CAS, Beijing, China, in 2006.

Currently, he is a Lecturer with the University of Electronic Science and Technology of China, Chengdu, China. His research interests are in the area of image processing and remote sensing applications.

Jianglin Ma received the B.S. degree in 2003 from the Xidian University, Xi'an, China, and the M.S. degree from the Institute of Remote Sensing Applications, CAS, Beijing, China, in 2006.

Currently, he is an Associate Researcher with Vrije Universiteit Brussel, Brussel, Belgium. His research interests are image processing and its application in remote sensing.